J. Synchrotron Rad. (1999). **6**, 1086–1095

YB_{66} – a new soft X-ray monochromator for synchrotron radiation. II. Characterization†

Joe Wong,[a]* T. Tanaka,[b] M. Rowen,[c] F. Schäfers,[d] B. R. Müller[d] and Z. U. Rek[c]

[a]Lawrence Livermore National Laboratory, University of California, PO Box 808, Livermore, CA 94551, USA, [b]National Institute for Inorganic Materials, 1-1 Namiki, Tsukuba, Ibaraki 305-0044, Japan, [c]Stanford Synchrotron Radiation Laboratory, PO Box 4349, Stanford CA 94309, USA, and [d]BESSY, Lentzallee 100, D-10587 Berlin, Germany. E-mail: wong@cmsl.llnl.gov

(*Received 23 December 1998; accepted 30 June 1999*)

YB_{66}, a complex boron-rich man-made crystal, has been singled out as a potential monochromator material to disperse synchrotron soft X-rays in the 1–2 keV region. Results of a series of systematic property characterizations pertinent for this application are presented in this paper. These include Laue diffraction patterns and high-precision lattice-constant determination, etch rate, stoichiometry, thermal expansion, soft X-ray reflectivity and rocking-curve measurements, thermal load effects on monochromator performance, nature of intrinsic positive glitches and their reduction. The 004 reflection of YB_{66} has a reflectance of ~3% in this spectral region. The width of the rocking curve varies from 0.25 eV at 1.1 keV to 1.0 eV at 2 keV, which is a factor of two better than that of beryl(1010) in the same energy range, and enables measurements of high-resolution XANES spectra at the Mg, Al and Si *K*-edges. The thermal bump on the first crystal arising from the low thermal conductivity of YB_{66} causes an energy drift of a few eVs with storage-ring current and necessitates periodic energy calibration with metal foils. The positive glitches in the transmission function just above the Mg *K*-edge have substantially been reduced using an Si or SiC mirror which suppresses the sharp reflectivity increases associated with anomalous scattering for the YB_{66} 006 reflection at the Y L_3- and L_2-edges. Continual operation over the past five years of a YB_{66} double-crystal monochromator installed on the JUMBO beamline at Stanford Synchrotron Radiation Laboratory (SSRL) indeed proves the long-term stability of this material in synchrotron radiation under ultrahigh vacuum conditions as indicated by the *invariance* in rocking-curve characteristics after being exposed to an accumulative power level of $\sim 3 \times 10^8$ J over this period of time.

Keywords: soft X-ray monochromators; YB_{66}; 1–2 keV spectroscopy.

1. Introduction

YB_{66}, a complex binary compound, has been singled out as a potentially useful soft X-ray monochromator for dispersing synchrotron radiation (Wong *et al.*, 1982, 1990). This material has a cubic crystal structure: space group $Fm3c$ (O_h^6), and contains over 1600 atoms per unit cell with a lattice parameter of 2.344 nm (Richards & Kasper, 1969). It is refractory and has a melting point of 2373 K. The material is semiconducting like silicon and germanium crystals and is expected to be stable to synchrotron radiation exposure. The strongest (400) reflection, with a $2d$ value of 1.172 nm, has a calculated Darwin width of <1 eV at 1–2 keV. There are no absorption edges of YB_{66} in this energy range (the Y L_3-edge being at 2080 eV and the B *K*-edge at 188 eV). Thus, YB_{66} satisfies all the X-ray and material property requirements for use as a soft X-ray monochromator in a synchrotron beam, particularly in the 1–2 keV region. The synthesis of high-quality single crystals of this material (Tanaka *et al.*, 1985; Kamimura *et al.*, 1993) opens up a new soft X-ray region (Rowen *et al.*, 1993; Schäfers *et al.*, 1992; Wong *et al.*, 1994; Tanaka *et al.*, 1994) not easily accessible before, for measuring the X-ray absorption spectra of Mg-, Al- and Si-bearing materials. The *K*-edge energies of these low-Z elements occur in the 1–2 keV region (Mg: 1303 eV; Al: 1559 eV and Si: 1839 eV) (Bearden & Burr, 1967). The *K*-spectra of these constituent elements in condensed matter, particularly the so-called XANES (X-ray absorption near-edge structure), involve predominently transitions to final *p*-states which are directly associated with the valence levels and are therefore diagnostic of the chemical bonding in terms of ligand electronegativity, coordination geometry, second or higher neighbour effects as well as the overall crystal structure (Wong *et al.*, 1994; Fröba, Wong, Behrens *et al.*, 1995; Fröba, Wong, Rowen *et al.*, 1995).

In the past few years a multi-laboratory collaborative developmental effort in crystal growth, topography,

† Part I. Wong *et al.* (1990).

rocking-curve measurements, soft X-ray reflectivity measurements, systematic homogeneity mapping, microprobe analysis, etch rates, and long-term stability in a synchrotron beam have been undertaken at NIRIM, BESSY, SSRL and LLNL. Data derived from these property characterizations have been used to understand various parameters controlling the crystal growth process as well as feedback information to improve and attain growth of *large and perfect* enough crystals for monochromator applications. In this paper the results of various characterization studies leading to the successful development of this novel soft X-ray monochromator material are presented.

2. Experimental

2.1. *Crystal growth and sample preparation*

Single crystals of YB_{66} have been grown by an indirect-heating floating zone (IHFZ) method. Since YB_{66} is a high-resistivity *p*-type semiconductor (Oliver & Brower, 1971) it is difficult to couple directly with induction heating of the order of a few hundred kHz. In the IHFZ process, which was developed specifically for the growth of YB_{66} single crystals (Tanaka *et al.*, 1985), the feed rod material is heated by radiation from an inductively heated tungsten ring placed between the feed rod and an RF work coil. Details of this crystal growth method (Tanaka *et al.*, 1985, 1990; Kamimura *et al.*, 1993) and subsequent refined procedures (Tanaka *et al.*, 1998) have been published elsewhere. In order to achieve the growth of high-quality single crystals for monochromator application, a number of growth parameters have been modified systematically based on feedback from characterization results obtained from X-ray topography, double-crystal diffraction analyses (rocking-curves width), and microprobe analysis of composition and impurities. These growth parameters include the number of zone passes, upward and downward drives, growth rate, rotation speed, RF power, and congruent and incongruent compositions. The highest quality currently achieved is represented by a full width at half maximum (FWHM) value of ~40 arcsec for the (10 0 0) rocking curve using Cu K_α radiation and asymmetrically cut Si(111) as a first crystal. This rocking-curve width is a factor of ~30 larger than the calculated value. The discrepancy may largely be due to crystal mosaicity, as well as defects and lattice deformations. In the soft X-ray region the measured FWHM values come much closer to the calculated values, within a factor of five or better.

In this work, extensive characterizations have been performed on a number of crystal boules. Both [001]- and [011]-oriented crystals have been grown with typical dimensions of 12 mm in diameter and 60 mm in length. (*a*) Crystals #6648 and #6652, which have a composition of [B]/[Y] = 62, were grown congruently in an upward drive mode at a growth rate of 12.5 mm h^{-1} and 25 mm h^{-1}, respectively. (*b*) Crystal #6716 was used for Laue diffraction using a tungsten source. (*c*) Crystal #6757, having a composition of [B]/[Y] = 56, was grown under an incongruent melting condition in which the composition of the molten zone is different from, and in equilibrium with, that of the growing crystal. This crystal has been used successfully as a soft X-ray double-crystal monochromator on the JUMBO beamline at SSRL since 1993. (*d*) Crystal #6825, in which 20 at% of Y was experimentally replaced by Sc in order to test whether such replacement can achieved high crystal quality during growth, was also used for flux measurements in a synchrotron beam.

The boules were sliced with a diamond saw parallel to the growth axis. The crystal quality deteriorated progressively at the zone end due to the large thermal gradient at the termination of the last zone pass. Approximately 10 mm from the zone ends was cut from the slices. Rectangular plates of YB_{66}, 12 mm by 25 mm and 1 mm thick, were used for monochromator crystals. The surfaces, parallel to the {100} planes, were first rough polished with B_4C powder followed successively with 9 μm and 3 μm diamond abrasives and a final polish with 1 μm Al_2O_3 powder on a tin polishing plate.

2.2. *Material characterizations*

A number of methods have been used to characterize the X-ray properties of the synthesized YB_{66} materials in terms of monocrystallinity, homogeneity in both chemical composition and diffraction properties, lattice constant, reflectivity in the 1–2 keV region, and materials properties such as thermal expansion, etch rate and stability in a synchrotron beam. These properties are pertinent to the use of this boron-rich material as a soft X-ray monochromator compatible with intense synchrotron radiation under ultrahigh vacuum conditions. The characterization methods may be laboratory-based and synchrotron-facility-based.

2.3. *Laboratory-based methods*

These include reflection Laue photographs to check for monocrystallinity, high-precision powder diffractometry for cell parameter determination, thermal expansion, microprobe analysis for composition and impurity distribution and etch rate. Details of the experimental aspects of these laboratory procedures will be described in conjunction with the respective results.

2.4. *Synchrotron-based methods*

White-light topographic measurements performed at SSRL and the corresponding results are described in detail elsewhere (Tanaka *et al.*, 1998). Reflectivity and energy resolution in the 1–2 keV region were preliminarily obtained using a reflectometer coupled to the double-crystal monochromator KMC beamline (Feldhaus *et al.*, 1986) at BESSY operated with an electron energy of 0.8 GeV and injection current of 540 mA. Monochromatic light from a double crystal of beryl(1010) was fed into the reflectometer chamber in which a YB_{66} crystal was mounted for reflectivity measurement as a function of the

incidence angle (*i.e.* θ–2θ scans), or as a function of photon energy at fixed Bragg and detector angles.

The rocking curves, transmission function of a *double-crystal* YB_{66} monochromator, and *K*-edge XAFS spectra of a variety of Si, Al and Mg model compounds were measured at the JUMBO beamline (Cerino *et al.*, 1984) at SSRL operated with an electron energy of 3 GeV, injection current of 100 mA and a lifetime of over 20 h. The beam size on the first YB_{66} crystal was 15 mm in the horizontal and 1.5 mm FWHM in the vertical. The horizontal flux density was essentially uniform. The vertical distribution was asymmetric due to toroidal mirror aberrations, *i.e. the smile*. The YB_{66} crystal pair was configured in a non-dispersive mode and with a fixed exit beam height, sending a monochromatic beam from the UHV monochromator chamber to the vacuum sample chamber (10^{-5} torr or better) through a 0.4 μm-thick CVD diamond window. The energy position of the monochromator was initially calibrated using its own transmission curve from the position of the L_3- and L_2-edges of Y at 2080 eV and 2156 eV (Bearden & Burr, 1967), respectively, assuming no chemical shift in YB_{66} from the metal values. X-ray absorption spectra were recorded by monitoring the total electron yield with a channeltron. The spot size on the sample was 2 mm (horizontal) × 1 mm (vertical). The integration time varies from 2 to 8 s point^{-1} dependent on elemental concentration of Si, Al or Mg in the spectral samples. Heat-load effects on the energy calibration of the double-crystal monochromator were also determined as a function of the SPEAR storage-ring current.

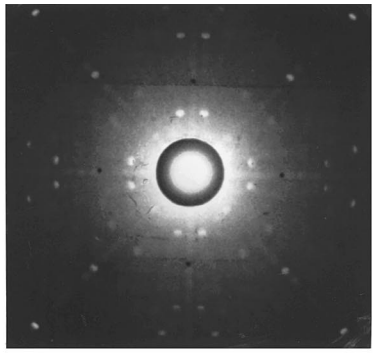

(*a*)

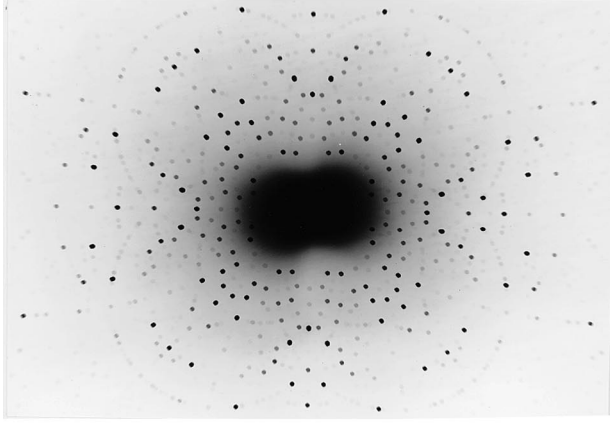

(*b*)

Figure 1
Laue photographs of YB_{66}(400) (*a*) taken in a back-reflection mode using a W source operated at 15 kV and 20 mA, and (*b*) taken with white light at SSRL.

3. Results and discussion

3.1. *Laue diffraction patterns and lattice constant*

Laue back-reflection diffraction was used to establish the monocrystallinity of the grown YB_{66} materials. Compared with earlier grown crystals (Oliver & Brower, 1971), which showed double spots (Wong *et al.*, 1990) indicative of twinning and subgrain structure, crystals grown by the IHFZ method are consistently of larger single-crystal domain. A Laue photograph taken with a tungsten tube source operated at 15 kV and 20 mA in a back-reflection mode is given in Fig. 1(*a*). Using 3000 ASA polaroid film, a sample-to-film separation of 1.5 cm and exposure time of 6 min were found to be optimal. A transmission Laue photograph taken on beamline 2–2 at SSRL is also shown in Fig. 1(*b*). Both exhibit a single-crystal pattern with the expected fourfold symmetry along the [001] direction.

A Guinier powder diffractometer using monochromatic Cu $K_{\alpha 1}$ radiation and high-purity Ge as an internal standard (a_0 = 0.5657906 nm) was employed to determine the lattice parameter of YB_{66}. Using an XLAT program to refine the 50 reflections observed in the Guinier powder diffraction pattern, values for the cell constant of 2.35052 nm and 2.34996 (21) nm were obtained (Rupp, 1988) for two adjacent slices from the same boule. The numbers in parentheses are the estimated standard deviations, σ, of the last significant digits. More recent work (Higashi *et al.*, 1997) yields the following cell constants of 2.34364 (6) nm and 2.34600 (9) nm for YB_{62} and YB_{56} using 551 and 534 independent reflections, respectively.

3.2. *Etch rate*

The room-temperature etch rate of YB_{66} in a caustic $K_3Fe_3(CN)_6$ solution was determined from weight-loss measurements as a function of time. The data are given in Fig. 2. An etch rate of 0.136 μm min^{-1} was determined from the slope of the weight loss *versus* time curve and known geometry of the YB_{66} crystals used. This linear etch rate is useful for controlled chemical removal of damaged surface layer due to cutting and mechanical abrasion.

3.3. *Stoichiometry and impurities*

Composition mapping on some selected grown YB_{66} crystals were performed using a Jeol electron microprobe spectrometer, model 733. Concentration profiles of Y, Al and Fe were mapped with a micrometre probe in two step-sizes: 100 μm steps and 2 μm steps over a region of 4–5 mm of the specimens. The latter two elements were suspected impurities introduced during grinding and ball milling of

Table 1
Microprobe analysis of Y, Al and Fe content (wt%) in YB_{66} single crystals.

Crystal	Position	Y	Al	Fe	Step size
#6652	Seed end	10.93 ± 0.18	0.11 ± 0.02	0.05 ± 0.01	40 steps, 100 μm apart
Disk *A*	Zone end	11.11 ± 0.26	0.10 ± 0.01	0.04 ± 0.01	40 steps, 100 μm apart
#6652	Seed end	11.19 ± 0.13	0.12 ± 0.02	0.05 ± 0.01	50 steps, 2 μm apart
Disk *B*	Zone end	11.21 ± 0.14	0.10 ± 0.01	0.03 ± 0.01	50 steps, 2 μm apart
#6648	Seed end	11.43 ± 0.19	0.40 ± 0.02	0.03 ± 0.01	40 steps, 100 μm apart
Disk *A*	Zone end	11.11 ± 0.26	0.43 ± 0.01	0.04 ± 0.01	40 steps, 100 μm apart
#6648	Seed end	11.14 ± 0.14	0.40 ± 0.03	0.03 ± 0.01	50 steps, 2 μm apart
Disk *B*	Zone end	11.18 ± 0.15	0.42 ± 0.02	0.04 ± 0.01	50 steps, 2 μm apart

the raw powder mixture in the course of synthesis of the feed rod material for the crystal growth. Two samples were analyzed: (i) sample #6652 with two discs cut one from the seed end and one from the zone end; (ii) sample #6648 with a rectangular slice cut along the growth axis. Two stepping modes were used in the microprobe measurements: (*a*) 40 points each 100 μm apart and (*b*) 50 points each 2 μm apart. The results are given in Table 1.

The standard deviation given in each entry in Table 1 is calculated from the 40 or 50 measurement points. There is no statistically significant variation in the concentration of Y along both crystals (cross sections in the case of #6652 and along the growth axis in the case of #6648). The theoretical wt% of Y in YB_{66}, YB_{64} and YB_{62} are 11.079, 11.386 and 11.71%, respectively. The stoichiometry of these two crystals derived from the microprobe analysis is $YB_{65\pm1}$. This value differs somewhat from that of $YB_{62\pm1}$ obtained by chemical analysis of both Y and B. The higher boron content may be due to surface sensitivity of the microprobe technique. The Al content is three to four times higher in #6648, whereas the Fe content is comparable in both samples. The microprobe data were used to advantage in minimizing both the Al and Fe impurity contents in subsequent powder preparations by (*a*) eliminating the use of alumina mortar and pestal and (*b*) removal of Fe using an HCl leach after the reacted feed rod material was pulverized in a stainless-steel ball mill.

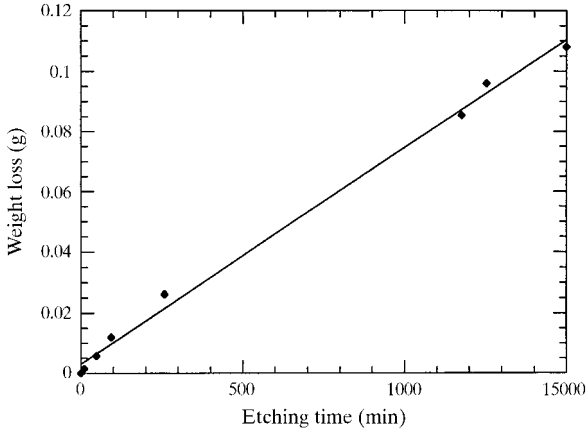

Figure 2
Weight loss of YB_{66} in a caustic potassium ferricyanide solution *versus* etching time.

3.4. *Thermal expansion coefficient*

Thermal expansion of YB_{66} was measured using a conventional dilatometer. A sample of dimensions ~6 mm × 6 mm × 15 mm was used. The long axis was parallel to the [100] direction. Since YB_{66} is a cubic crystal, the thermal expansion is isotropic, independent of crystal orientation. The linear expansion coefficients were obtained from the first derivatives of the measured thermal expansion curve plotted as a function of temperature. The results are plotted in Fig. 3. Least-squares analysis of the data yield a linear temperature dependence given by α = 3.521 + 0.01255 T with a correlation factor of 0.998. Together with a shift in Bragg angle, this data will be used to determine the temperature of the first crystal in a double-crystal set-up.

3.5. *Rocking curves at Mg K_α energy (1.2536 keV)*

Rocking-curve measurement at the Mg K_α (1.2536 keV) is a direct characterization of YB_{66} for use as a soft X-ray monochromator in the 1–2 keV region. This was performed in a vacuum spectrometer using a θ–2θ geometry with the Mg anode operated at 2.5 kV and 10 mA. Source divergence was 1.3 mrad. A proportional counter, operated at +1410 V and using a P-50 gas (50% Ar + 50% methane) at 200 torr was used as the detector. Beryl(1010) was used as the first crystal and the YB_{66} (400) samples as the second crystal. In Fig. 4 the rocking curves of sample #6648 cut along the growth axis are plotted as a function of position

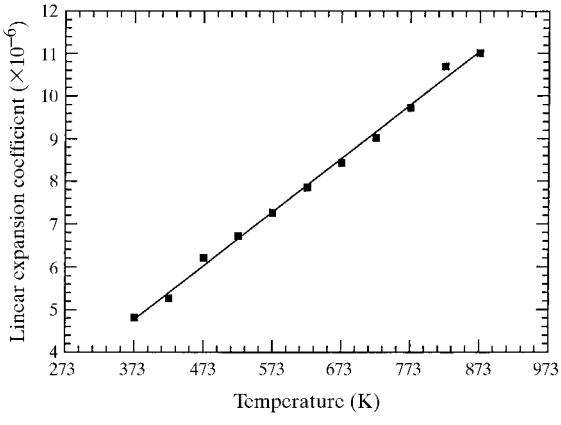

Figure 3
Linear expansion coefficient of YB_{66} as a function of temperature.

(in mm) from the seed end to the growth end. Single symmetric rocking curves are obtained to ~21 mm from the seed end, beyond which the rocking curve broadens with the appearance of a shoulder at 26 mm and a discernible second peak at 29 mm, indicative of a sub-grain boundary at the growth end. It is evident that the (single) crystal quality degrades from the seed end towards the growth end.

3.6. *BESSY data*

3.6.1. *Absolute reflectivity.* The absolute reflectance and energy resolution of YB_{66} (sample #6757) has been measured as a function of photon energy in the 1–2 keV region using the KMC reflectometer (Kühne & Müller, 1989) at BESSY. The reflectance and energy resolution (FWHM) are shown in Figs. 5(*a*) and 5(*b*). The resolution data were not deconvoluted with respect to the performance of the incoming light beam because of insufficient knowledge of the resolution and beam divergence in the reflectometer. However, direct comparison with similar measurements on a beryl(1010) crystal shows that the energy resolution of YB_{66} is at least a factor of two better. The laboratory measurement with Mg K_α radiation is in good agreement with this synchrotron data as shown by the open triangle points at 1.254 keV plotted also in Figs. 5(*a*) and 5(*b*). The result of an energy scan at fixed Bragg angle (open circles at 1.4 keV) yielded an identical result. The peak reflectivity of YB_{66} is of the order of a few percent with a broad plateau at ~3.5% between 1.3 and 1.7 keV. It is worth noting that the reflectivity and energy resolution of YB_{66} is a smooth function of photon energy, while those of beryl ($Al_2Si_6Be_3O_{18}$) exhibit structures about the Al and Si *K*-absorption edges at 1.54 keV and 1.84 keV, respectively.

3.6.2. *Spatial uniformity.* To check for spatial uniformity, the reflectivity was also measured at a fixed photon energy of 1.7 keV as a function of position along the growth axis from the seed end to the zone end. The data in Fig. 6 exhibit a constant reflectance value of $3.1 \pm 0.1\%$ across a length of ~17 mm; the corresponding Bragg angle, however, exhibits a monotonic decrease from 51.035° to 50.980° in the same region, indicative of an increase in lattice constant from the seed end to the zone end. The increase in a_0 is attributable to composition variation towards the zone end in the crystal.

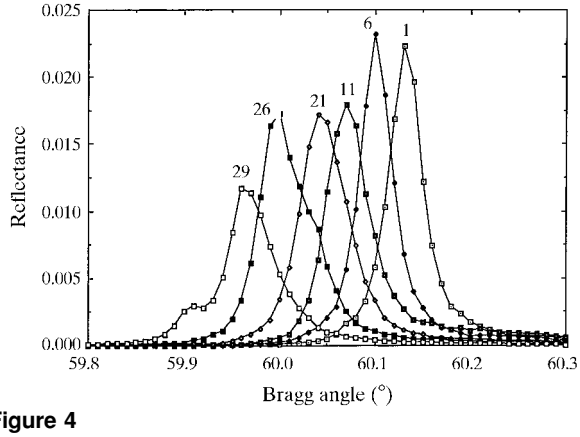

Figure 4
One-crystal rocking curves of sample #6648 YB_{66}(400) at the Mg K_α energy as a function of distance from the seed end. The number on each curve denotes the distance in mm from the seed end.

3.7. *JUMBO data*

3.7.1. *Double-crystal rocking curves.* The full width at half maximum (FWHM) of the double-crystal rocking curves plotted for two pairs of YB_{66} crystals and compared with those for beryl(1010), InSb(111) and quartz(1010) as a function of energy is shown in Fig. 7. Although YB_{66} crystal #6825 (Sc doped) has significantly higher resolution than crystal #6757, it was unintentionally contaminated with iron from the milling of the feed materials. Iron fluorescence from this crystal pair was unacceptable in an operational monochromator. Crystal #6757 is more typical of the resolution observed, the FWHM of which monotonically increases from ~0.25 eV at 1100 eV to ~0.5 eV at 1500 eV and ~1.0 eV at 2000 eV just below the Y L_3-edge where the reflectivity drops sharply. Both beryl and InSb have lower resolution than YB_{66}, while that of quartz is much higher. The use of quartz as a monochromator for high-intensity

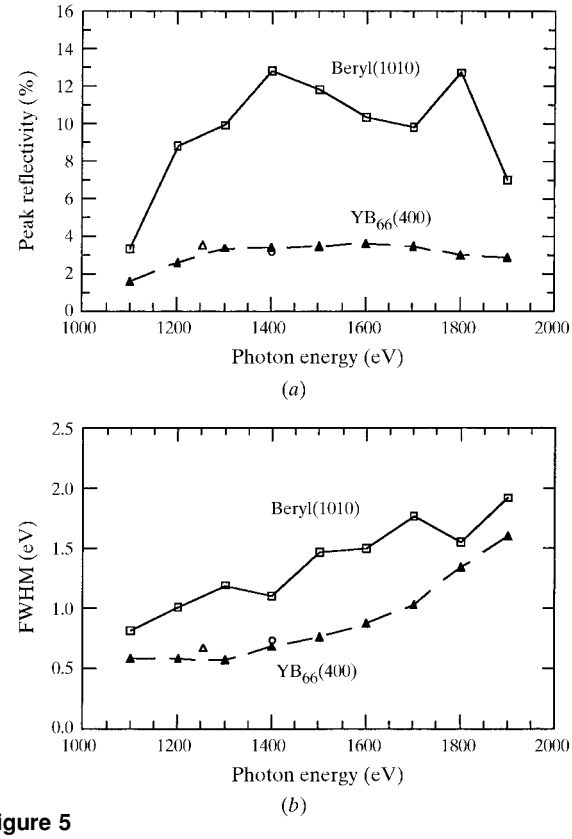

Figure 5
Comparison of (*a*) reflectance and (*b*) FWHM of YB_{66}(400) and beryl(1010) in the 1–2 keV region from single-crystal rocking curves measured on the KMC line at BESSY. The open triangles correspond to the Mg K_α data and the open circles were obtained from an energy scan at fixed Bragg angle at 1.4 keV. The data have not been corrected for divergence of the incident light.

synchrotron radiation is limited in two ways. First, it damages very rapidly in the white synchrotron beam. The *radiation damaged* curve in Fig. 7 is for the case after only several days use with the stored current in SPEAR of <50 mA. Second, the useful energy range of quartz is rather limited from 1500 eV [due to the 2*d* value of quartz(1010) reflection] to the Si *K*-edge at 1840 eV.

This resolution from the YB_{66} crystals in the 1–2 keV region is quite suitable for recording relatively high-resolution *K*-edge XANES spectra for Mg, Al and Si as shown in a later section. Above 2 keV the Y $L_{3,2,1}$-edges set in at 2080, 2156 and 2373 eV, respectively, and lower the transmission function of YB_{66} substantially, making it less attractive for use at higher photon energies when compared with available higher-*Z* monochromator materials such as Ge and InSb (Fig. 8).

3.7.2. *Thermal load.* YB_{66} is known to have a low thermal conductivity, similar to those of glassy materials (Slack & Oliver, 1971). The performance of the monochromator can be strongly influenced by the thermal load on the first crystal (which 'sees' a white beam from the synchrotron) in a double-crystal set-up, particularly with white radiation from a hard X-ray storage ring such as SPEAR. The temperature of the first crystal may be determined by measuring the deviation of its Bragg angle with respect to the second crystal (fixed) as a function of Bragg angle. The measured angular shift combined with the known lattice expansion of YB_{66} (shown in Fig. 3) have been used to determine the temperature of the first crystal. In Fig. 9 the temperature of the first crystal is plotted as a function of Bragg angle for two incident power levels: ~22 W and <1 W. The latter power level was facilitated by use of a 25 μm Al filter upstream from the monochromator. At low power a steady temperature of ~333 K is attained at a Bragg angle of 60°. The fluctuation at low angle is due primarily to low signal level. At higher thermal load, the temperature of the first crystal increases progressively from 473 to 637 K at higher Bragg angle. The temperature increase with Bragg angle is basically due to an increase in thermal load per unit area on the crystal as a result of a reduction of the beam footprint on the first crystal.

The lattice expansion of the first crystal under the thermal load induces an energy shift which varies monotonically with the storage-ring current. In Fig. 10 a calibration curve using the first inflexion point (given by the first maximum in the first derivative spectrum) in the Al metal *K*-edge spectrum defined at 1559 eV (Bearden & Burr, 1967) can be determined as a function of SPEAR current. Data above 50 mA correspond to the normal mode

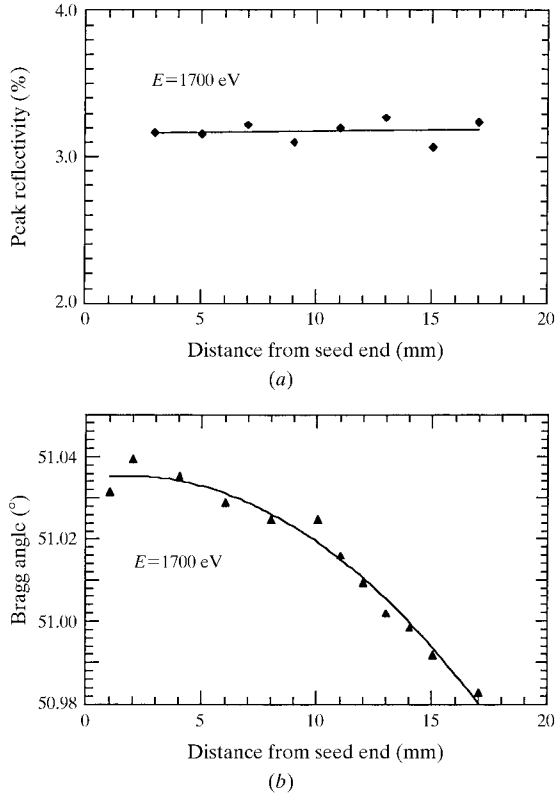

Figure 6
(*a*) Reflectance and (*b*) Bragg angle of sample #6757 YB_{66}(400) at 1700 eV as a function of distance from seed end.

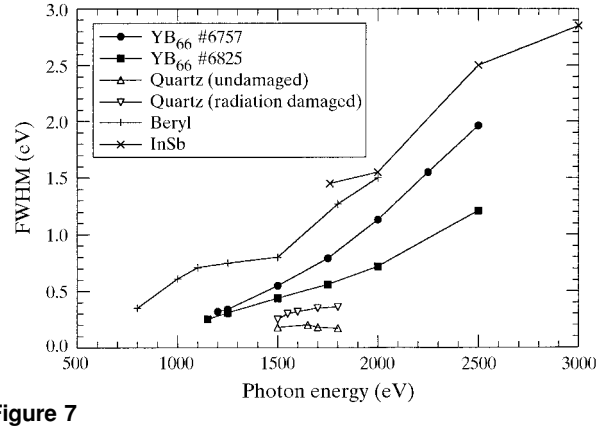

Figure 7
FWHM of double-crystal rocking curves as a function of photon energy for two YB_{66} crystals #6767 and #6824 (Sc doped), and comparison with those for quartz (undamaged and damaged), beryl and InSb.

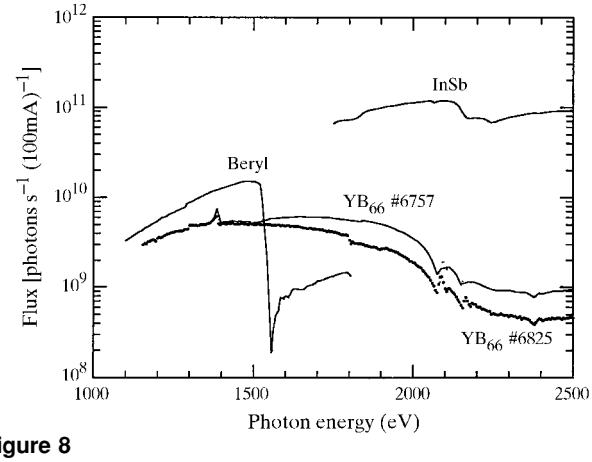

Figure 8
Flux throughput of various double-crystal monochromators in the 1–2.5 keV region.

for multibunch operation and those below 40 mA correspond to a timing mode for single-bunch operation. Thus, at the Al *K*-edge the energy calibration varies by 2–3 eV between fills and must be corrected for if accurate edge-shift data are desirable. Energy shifts at the Mg *K*-edge and Si *K*-edge as a function of SPEAR current are also comparable.

Compared with highly perfect Si crystals and other semiconducting monochromator materials such as Ge and InSb, the spatial uniformity of individual YB_{66} crystals as seen in the data given in Figs. 5 and 6 is thus far limited to, at best, 2–3 cm in length. Therefore, in a double-crystal monochromator set-up, the relative locations in each of the crystal pair used for monochromatization is very important and have to be mapped out carefully for optimal performance in terms of both flux throughput and energy resolution. Such mapping using hard X-ray topography has indeed been performed for the C1/C2 YB_{66} pair (crystal #6757) before installing on the JUMBO beamline at SSRL. Furthermore, the FWHM of the rocking curve at 1500 eV has also been mapped as a function of beam position on the second crystal at various beam positions on the first crystal (Fig. 11). Thus, in routine XAFS scans, both the 'angular' phase (Bragg angle) and 'translational' phase between the two crystals must be optimized as a function of photon energy range intended for the scan.

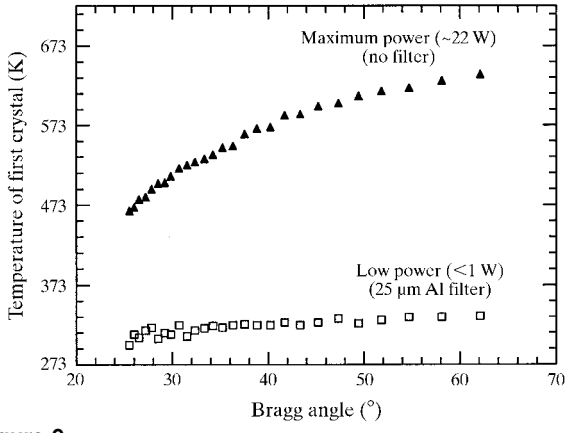

Figure 9
Temperature of the first crystal of a double-crystal YB_{66} monochromator (the C1/C2 pair from sample #6757) on the JUMBO beamline at SSRL with SPEAR operating at 3 GeV electron energy plotted as a function of Bragg angle at two estimated thermal power levels.

3.7.3. *Positive glitches*. Careful examination of the flux data presented in Fig. 8 reveals that there are two positive glitches in the transmission function of YB_{66} at 1385.6 and 1438 eV in the double-crystal configuration. These glitches limit the usefulness of YB_{66} for spectroscopy in the region just above the Mg *K*-edge at 1303 eV (Fig. 12). For the case of dilute specimens where the ratio of sample signal to incident signal is small, these glitches do not normalize out and interfere strongly with analysis of both the XANES and EXAFS data.

The nature of these glitches has been elucidated using a combination of photoemission experiments, reflectivity measurements and anomalous scattering calculations (Tanaka *et al.*, 1997). They are now understood to be due to the transmission at an energy 1.5 times higher than the 004 reflection and correspond to the Y L_3- and L_2-absorption edges at 2080 and 2156 eV, respectively. Reflectivity measurements and structure-factor calculations for the 006 reflection confirmed that these glitches are caused by the sharp reflectivity increases associated with anomalous scattering for the 006 reflection at the Y L_3- and L_2-edges. To minimize the intensity of the anomalous high harmonics at the glitches, a cut-off mirror is used. Reflections from an Si or SiC surface will have a sharp cut-off for the Si *K*-absorption edge at 1839 eV. For example, the calculated reflectivity for an SiC mirror at a glancing angle of 1.25° is over 80% below 1480 eV, but only 5% at 2080 eV. This was realized by the installation of an SiC mirror downstream from the YB_{66} monochromator on JUMBO. Fig. 13 shows the relative intensity of the flux in the region of the glitches

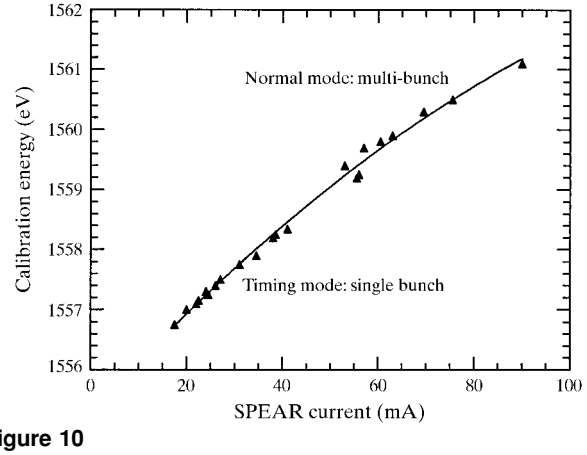

Figure 10
Calibration energy of the C1/C2 double-crystal YB_{66} monochromator at the Al *K*-edge (1559 eV) as a function of SPEAR current.

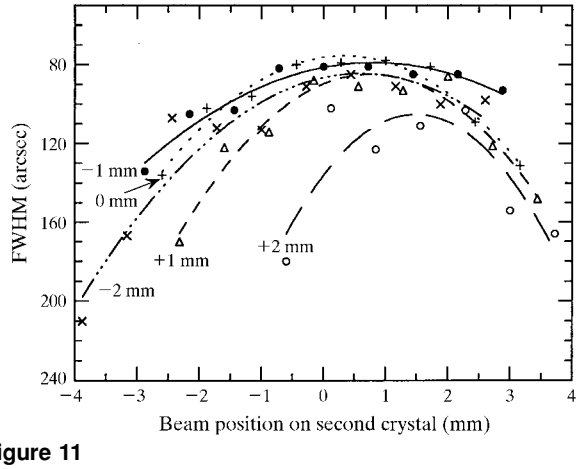

Figure 11
Rocking-curve width of the C1/C2 monochromator as a function of beam position on the second crystal at various positions of the beam on the first crystal as labelled on each curve.

and their suppression as a function of glancing angle of the beam on the mirror. The data show that at 1.38° most of the higher-order flux due to the glitches is eliminated without substantial reduction of the transmission at the energy of interest. Fig. 14 shows the Mg *K*-edge spectra of a series of Mg-bearing materials ranging from yoderite [$Mg_2Al_{5.3}Fe_{0.5}Ca_{0.2}Si_4O_{17.6}(OH)_{2.4}$], diopside ($MgCaSi_2O_6$), $MgSiN_2$ to $MgTiO_3$ recorded with (right-hand panels in Fig. 14) and without (left-hand panels in Fig. 14) the SiC cut-off mirror at a glancing angle of 1.25°. This series of Mg compounds is chosen to illustrate the effectiveness of the cut-off mirror in suppressing the two positive glitches as a function of increasing Mg content from yoderite to $MgTiO_3$.

4. Concluding remarks

The collaborative efforts in crystal growth, topographic evaluation and material characterization described in this work, together with an interactive feedback between these research areas, have led to a successful development of YB_{66} as a soft X-ray monochromator for synchrotron radiation. Since the first installation of a double-crystal YB_{66} monochromator (Rowen *et al.*, 1993), continual operation on the JUMBO beamline at SSRL over the past five years has proved that this boride material is synchrotron-radiation stable under UHV conditions as shown by the *invariance* in rocking-curve characteristics after being exposed to an accumulative radiation power of $\sim 3 \times 10^8$ J over this period of time. This capability opens a new spectroscopic window to investigate low-*Z* materials containing Si, Al and Mg with XAFS. In Fig. 15 the *K*-edge of some selected Si, Al and Mg model compounds are plotted and show systematic edge shift and increase in white-line intensity of the $1s \rightarrow 3p$ transition as a function of ligand type, electronegativity and coordination number. For the Si compounds, except for stishovite, which is a high-pressure form of silicon dioxide, all have Si in fourfold coordination by the respective ligands in the crystal structure. In Al_4C_3 and AlN, the Al is in fourfold coordination, whereas in Al_2O_3 and AlF_3 it is sixfold coordinated. In $MgSiN_2$, MgO and pyrope, a Mg-bearing garnet, the Mg coordination is 4, 6 and 8, respectively. Again, the XANES spectra exhibit systematic positive edge shift together with a progressive white-line intensity increase. Furthermore,

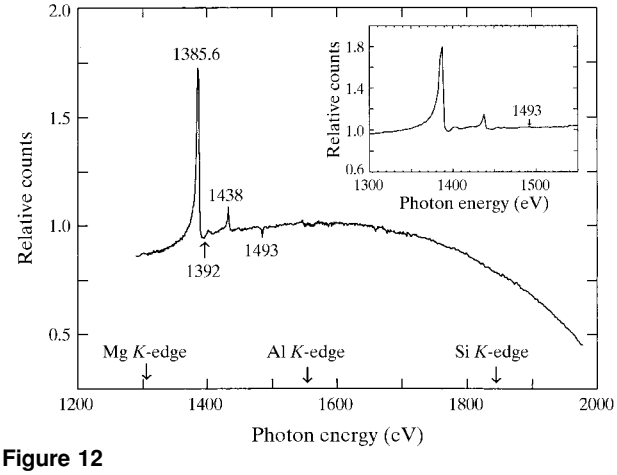

Figure 12
Glitches in the transmission function of a double-crystal $YB_{66}(400)$ monochromator above the Mg *K*-edge. The inset shows the corresponding transmission function with a 45° azimuthal rotation of the YB_{66} crystals, showing the disappearance of the negative glitch at 1439 eV and the persistence of two positive ones.

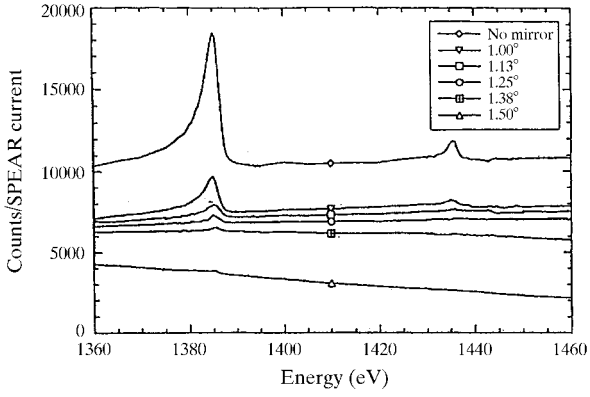

Figure 13
Reduction of the 006 glitches with increasing glancing angle of an SiC cut-off mirror located downstream from the YB_{66} double-crystal monochromator.

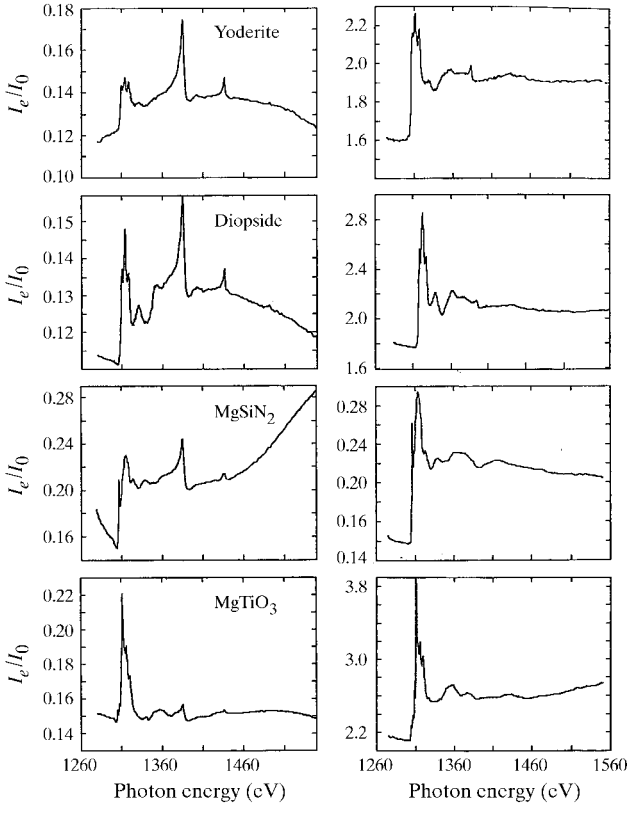

Figure 14
Mg *K*-edge spectra of yoderite, diopside, $MgSiN_2$ and $MgTiO_3$ recorded without (left-hand panels) and with (right-hand panels) the SiC cut-off mirror to suppress the two positive glitches at 1385.6 and 1438 eV.

the transmission function of YB_{66} permits a large energy scan of the XAFS spectrum for both Mg and Al, thus permitting larger *k*-range data for Fourier transform analysis (Wong *et al.*, 1994).

L- and *M*-edge spectroscopy of many of the 4*p* elements and rare-earths are now possible with the use of the YB_{66} monochromator since their respective edge energies are in the 1–2 keV region, as illustrated in Fig. 16. An example is given for the case of the Br $L_{3,2}$ spectra of an ionic compound KBr and $KBrO_3$ in which the formal valence of Br is +5 in the bromate ion. The $L_{3,2}$ spectra of Br in the two compounds are quite distinct and characteristic of their chemical and structural environment.

The availability of intense monochromated photons in the 1–2 keV region of the electromagnetic spectrum will no doubt impact a variety of disciplines such as materials science, mineralogy, catalysis, metallurgy, environmental and biosciences. Analysis and understanding of the model Si, Al and Mg compound systems have begun to shed light on more complex materials containing these constituent elements in a variety of aluminosilicate materials. These include zeolites, which are open three-dimensional aluminosilicates important as catalysts in petroleum cracking and other chemical syntheses; clay minerals important in geoscience, soil chemistry and environmental clean-up; aluminium alloys important in hi-tech structural components; Mg centres important in novel catalysts and in biomolecules; and, of course, silicon-based materials relevant to the semiconductor industry. Results obtained thus far on Si, Al and Mg model compounds (Wong *et al.*, 1994; Fröba, Wong, Behrens *et al.*, 1995; Fröba, Wong, Rowen *et al.*, 1995; Wong *et al.*, 1997) indeed reveal a wealth of fine-structure features in the XANES spectra that may be systematically correlated with the bonding, local coordi-

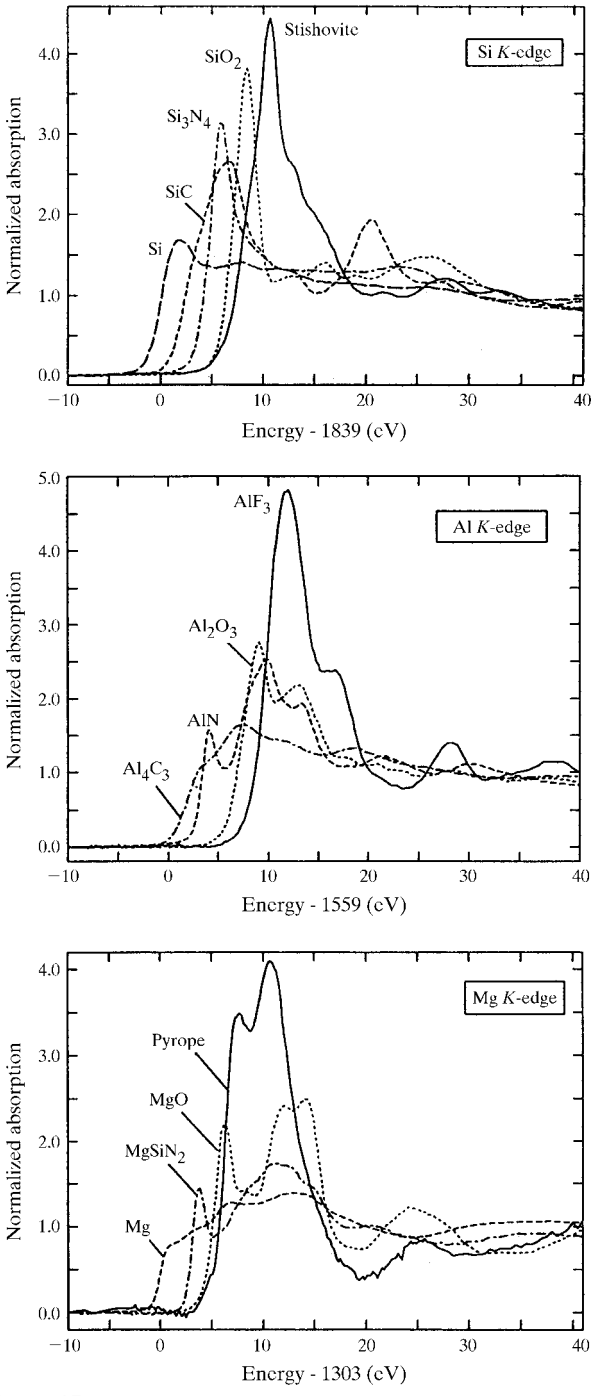

Figure 15
Normalized *K*-edge XANES spectra of selected Si, Al and Mg model compounds showing systematic edge shift and increase of white-line intensity of the $1s \rightarrow 3p$ transition as a function of ligand type (electronegativity) and coordination number.

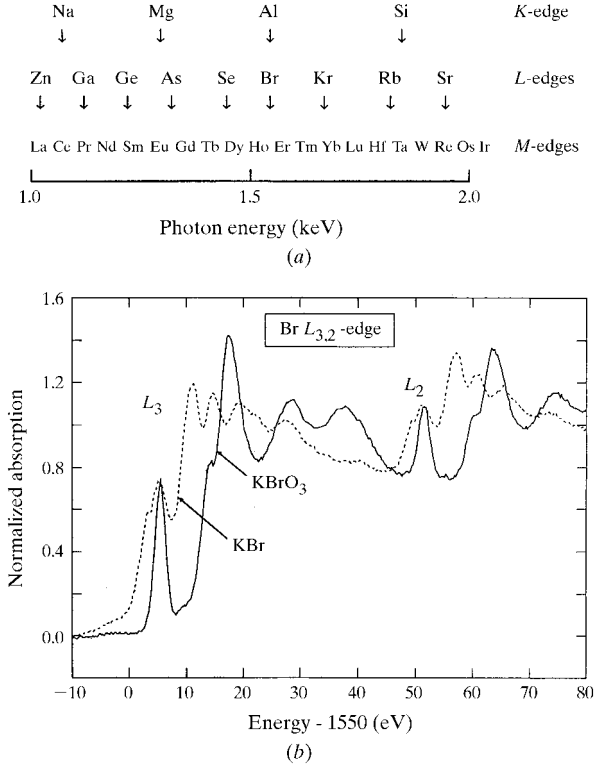

Figure 16
(*a*) List of elements with *L* and *M* absorption edges in the 1–2 keV region. (*b*) Normalized $L_{3,2}$-edge XANES of Br in KBr and $KBrO_3$ showing the richness of the spectral features with bonding and structure of Br in each of the compounds.

nation, type of neighbouring atoms as well as bond angle about the central atom. Successful installations of the YB_{66} monochromator have also been reported recently at the SRS facility in Daresbury, UK (Smith *et al.*, 1998), and the UVSOR facility in Okazaki, Japan (Kinoshita *et al.*, 1998).

This work is in part performed under the auspices of the US Department of Energy (DOE) by the Lawrence Livermore National Laboratory under contract W-7405-ENG-48. SSRL is funded by DOE, Office of Basic Energy Sciences. We are thankful for the single-bunch data supplied by Graham George and high-precision lattice-constant measurements by P. Rogl. JW is also grateful for partial support for this research by the Science and Technology Agency, Japan, and the Alexander von Humboldt Foundation, Germany.

References

Bearden, J. A. & Burr, A. F. (1967). *Rev. Mod. Phys.* **39**, 125–196.
Cerino, J., Stöhr, J., Hower, N. & Bachrach, R. (1984). *Nucl. Instrum. Methods*, **172**, 227–231.
Feldhaus, J., Schaefers, F. & Peatman, W. B. (1986). *Proc. SPIE*, **733**, 242–247.
Fröba, M., Wong, J., Behrens, P., Sieger, P., Rowen, M., Tanaka, T., Rek, Z. & Felsche, J. (1995). *Physica B*, **208**, 65–69.
Fröba, M., Wong, J., Rowen, M., Brown, G. E. Jr, Tanaka, T. & Rek, Z. (1995). *Physica B*, **208**, 555–559; *MRS Sym. Proc.* **371**, 100–104.
Higashi, I., Kobayashi, K., Tanaka, T. & Ishizawa, Y. (1997). *J. Solid State Chem.* **133**, 16–20.
Kamimura, Y., Tanaka, T., Otanie, S., Ishizawa, Y., Rek, Z. & Wong, J. (1993). *J. Cryst. Growth*, **128**, 429–436.
Kinoshita, T., Takata, Y., Matsukawa, T., Aritani, H., Matsuo, S., Yamamoto, T., Takahashi, M., Yoshida, M., Yoshida, T., Ufuktepe, Y., Nath, K. G., Kimura, S. I. & Kitajima, Y. (1998). *J. Synchrotron Rad.* **5**, 726–729.
Kühne, M. & Müller, P. (1989). *Proc. SPIE*, **1140**, 220–224.
Oliver, D. W. & Brower, G. D. (1971). *J. Cryst. Growth*, **11**, 185–190.
Richards, S. M. & Kasper, J. S. (1969). *Acta Cryst.* B**25**, 237–251.
Rowen, M., Rek, Z., Wong, J., Tanaka, T., George, G. N., Pickering, I. J., Via, G. H. & Brown, G. E. Jr (1993). *Synchrotron Rad. News*, **6**(3), 25–28.
Rupp, B. (1988). *Scr. Metall.* **22**, 1–3.
Schäfers, F., Müller, B. R., Wong, J., Tanaka, T. & Kamimura, Y. (1992). *Synchrotron Rad. News*, **5**, 28–29.
Slack, G. A. & Oliver, D. W. (1971). *Phys. Rev. B*, **4**, 1714–1719.
Smith, A. D., Cowie, B. C., Sankar, G. & Thomas, J. M. (1998). *J. Synchrotron Rad.* **5**, 716–718.
Tanaka, T., Aizawa, T., Rowen, M., Rek, Z., Kitajuma, Y., Higashi, I., Wong, J. & Ishizawa, Y. (1997). *J. Appl. Cryst.* **30**, 87–91.
Tanaka, T., Ishizawa, Y., Wong, J., Rek, Z., Rowen, M., Schäfers, F. & Müller, B. R. (1994). *Jpn. J. Appl. Phys.* **10**, 110–113.
Tanaka, T., Otani, S. & Ishizawa, Y. (1985). *J. Cryst. Growth*, **73**, 31–40.
Tanaka, T., Otani, S. & Ishizawa, Y. (1990). *J. Cryst. Growth*, **99**, 994–998.
Tanaka, T., Rek, Z., Wong, J. & Rowen, M. (1998). *J. Cryst. Growth*, **192**, 141–147.
Wong, J., Froba, M., Tamura, E., Rowen, M., Rek, Z. & Tanaka, T. (1997). *J. Phys. IV France*, C**2**, 511–515.
Wong, J., George, G. N., Pickering, I. J., Rek, Z., Rowen, M., Tanaka, T., Via, G. H., DeVries, B., Vaughan, D. E. W. & Brown, G. E. Jr (1994). *Solid State Commun.* **92**(7), 559–563.
Wong, J., Roth, W. L., Batterman, B. W., Berman, L. E., Pease, D. E., Heald, S. & Barbee, T. W. (1982). *Nucl. Instrum. Methods*, **195**, 133–139.
Wong, J., Shimkaveg, G., Goldstein, W., Eckart, M., Tanaka, T., Rek, Z. & Tompkins, H. (1990). *Nucl. Instrum. Methods*, A**291,** 243–248.